Heterogeneous Catalysis

DOI: 10.1002/ange.201407785

Efficient Coupling of Solar Energy to Catalytic Hydrogenation by Using Well-Designed Palladium Nanostructures**

*Ran Long, Zhoulv Rao, Keke Mao, Yu Li, Chao Zhang, Qiliang Liu, Chengming Wang, Zhi-Yuan Li, Xiaojun Wu, and Yujie Xiong**

Abstract: *A Ru^{3+}-mediated synthesis for the unique Pd concave nanostructures, which can directly harvest UV-to-visible light for styrene hydrogenation, is described. The catalytic efficiency under 100 $mW\,cm^{-2}$ full-spectrum irradiation at room temperature turns out to be comparable to that of thermally (70 °C) driven reactions. The yields obtained with other Pd nanocrystals, such as nanocubes and octahedrons, are lower. The nanostructures reported here have sufficient plasmonic cross-sections for light harvesting in a broad spectral range owing to the reduced shape symmetry, which increases the solution temperature for the reaction by the photothermal effect. They possess a large quantity of atoms at corners and edges where local heat is more efficiently generated, thus providing active sites for the reaction. Taken together, these factors drastically enhance the hydrogenation reaction by light illumination.*

Catalytic hydrogenation includes a large group of addition reactions of hydrogen to unsaturated bonds, which is among the simplest transformations in organic chemistry and has been extensively involved in various chemical processes.[1,2] The typical heterogeneous catalysts for hydrogenation are commonly made of noble metals and their alloys, among which Pd is a widely used one given its strong interactions with molecular hydrogen (H_2).[3–7] Like other catalytic reaction systems,[8–12] the activities of Pd nanocrystals in hydrogenation are highly dependent on their surface structures.[13] Thus structure control holds the promise for tuning their catalytic performance in hydrogenation reactions. In addition to the reaction activities of catalysts, the energy source is another important parameter for catalytic reactions.

To meet energy and environmental demands, it would be ideal to utilize solar energy instead of heat to drive the organic reactions. For this reason, attempts have been made to couple the solar energy with various catalytic organic reactions, by utilizing the surface plasmon properties of metal nanocrystals.[14–17] Nevertheless, hydrogenation reactions are mostly performed with thermal energy or/and under high pressure. To efficiently couple solar energy to reactions, the catalytic nanocrystals (e.g., Pd as the most active metal for hydrogenation) should have sufficient plasmonic cross-sections for light harvesting in a relatively broad spectral range.

The Pd nanoparticles which are synthesized in solution phase, however, generally have small sizes below 10 nm, which confines their plasmonic band to the UV spectral range with very small optical cross-sections.[18] To tune their plasmonic band for longer wavelengths, one can increase the particle sizes, mostly through a seeding growth process.[19,20] Such a seeding scheme requires low concentrations of metal precursors to avoid homogeneous nucleation, thus constituting an obstacle to large-scale synthesis. In addition to size control, intuitively the plasmonic band can be expanded to the visible spectral region by lowering the shape symmetry of nanocrystals,[21] which in turn absorbs light at a wide range of wavelengths. Complex nanostructures such as concave nanocubes represent such a class of geometries. The concave nanostructures also possess a large number of atoms at corners and edges, which are are generally believed to be active sites for hydrogenation,[13] and have thus become our focus for a model system. Taken together, the concave nanostructures with large particle sizes would be ideal candidates as plasmonic-driven catalysts for hydrogenation.

Herein, we report a facile Ru^{3+}-mediated direct synthesis for Pd nanostructures with well-defined concave shapes and particle sizes of up to 40 nm. The nanostructures exhibit a plasmonic band covering the UV-to-visible spectral range, which thus induces higher temperature to sustain styrene hydrogenation through photothermal effect. In reference to Pd nanocubes and octahedrons with comparable sizes, our Pd nanostructures show dramatically enhanced catalytic activities in styrene hydrogenation under full-spectrum illumina-

[*] Dr. R. Long,[+] Z. Rao,[+] K. Mao, Y. Li, Q. Liu, Dr. C. Wang, Prof. X. Wu, Prof. Y. Xiong
Hefei National Laboratory for Physical Sciences at the Microscale
Collaborative Innovation Center of Chemistry for Energy Materials
School of Chemistry and Materials Science and
CAS Key Laboratory of Materials for Energy Conversion
University of Science and Technology of China
Hefei, Anhui 230026 (P. R. China)
E-mail: yjxiong@ustc.edu.cn
Homepage: http://staff.ustc.edu.cn/~yjxiong/
C. Zhang, Prof. Z.-Y. Li
Laboratory of Optical Physics, Institute of Physics
Chinese Academy of Sciences, Beijing 100190 (P. R. China)
Prof. Z.-Y. Li
College of Physics and Optoelectronics
South China University of Technology
Guangzhou 510641 (P. R. China)

[+] These authors contributed equally to this work.

[**] This work was financially supported by the NSFC (No. 21101145, 91123010), Recruitment Program of Global Experts, CAS Hundred Talent Program, Specialized Research Fund for the Doctoral Program of Higher Education (No. 20123402110050), and Fundamental Research Funds for the Central Universities (No. WK2060190025, WK2060190037).

Supporting information for this article (Ru^{3+}-mediated synthesis of Pd nanostructures, styrene hydrogenation, sample characterizations, and computational methods) is available on the WWW under http://dx.doi.org/10.1002/anie.201407785.

tion at room temperature, thus approaching the yield of reactions which are thermally heated at 70 °C. Using the thermal reaction as a benchmark, we found that the sharp corners and edges of our Pd nanostructures may make important contributions to the performance improvement through local heat generation.

Our materials synthesis is performed by simply introducing a certain amount of $RuCl_3$ into the well-established protocol for Pd nanocubes. The protocol for Pd nanocubes involves K_2PdCl_4 as a metal precursor, poly(vinyl pyrrolidone) (PVP) as a stabilizer, ascorbic acid as a reductant, and KBr as a capping agent to promote {100} facets.[22] As displayed in Figure 1 a, such a protocol in the absence of $RuCl_3$ typically produces Pd nanocubes with sharp corners and edges with sizes of about 18 nm. As $RuCl_3$ is added into this synthesis, the morphologies of the resulting products are significantly altered (see Figure 1 b,c and Figure S1 in the Supporting Information): 1) the particle sizes are increased from 18 nm to 50 nm, and 2) the structures gradually become more complex to reduce shape symmetry as $RuCl_3$ concentration increases. Notably, the products obtained in the presence of 5.0 mg $RuCl_3$ have a profile analogous to concave structures with an average edge length of 40 nm and enclosed by {730} facets (Figure 1 d, namely concave nanostructures in this work).

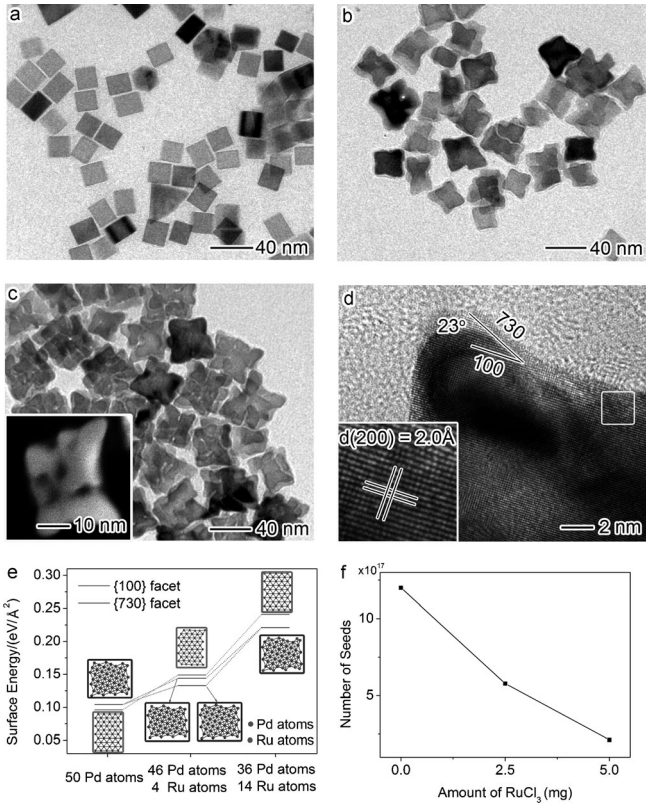

Figure 1. Transmission electron microscopy (TEM) images of Pd nanostructures obtained in the presence of different amounts of $RuCl_3$: a) 0 mg, b) 2.5 mg, and c) 5.0 mg. The ICP-MS measurements show that all the samples do not contain elemental Ru. The inset of (c) shows the scanning TEM (STEM) image of a nanocrystal. d) High-resolution TEM (HRTEM) image of a nanocrystal in (c). e) Computed surface energies of pristine Pd{100} and Pd{730} and those with certain Pd atoms substituted by Ru atoms. The specific values are listed in Table S1. f) Plot showing the number of seeds (i.e., particles) versus the concentration of $RuCl_3$ added to the syntheses in (a–c). The numbers of seeds are calculated based on the atomic concentrations (measured by ICP-MS) and particle sizes of products.

Although seeding methods have been reported for similar Pd concave nanostructures,[23,24] the direct synthesis presented here not only simultaneously controls particle size and structure to the desired regime, but also enables the production of nanostructures with about 20 times larger quantity. Upon recognizing the effect of $RuCl_3$ on final products, we are in a position to investigate what role the $RuCl_3$ plays in inducing the changes in particle size and structure. We employed inductively coupled plasma mass spectrometry (ICP-MS), X-ray diffraction (XRD; see Figure S2), and energy-dispersive X-ray spectroscopy (EDS; see Figure S3) to extensively characterize the sample in Figure 1 c, and all show the absence of elemental Ru. Note that X-ray photoelectron spectroscopy (XPS) is incapable of examining trace Ru as its characteristic $3d_{5/2}$ and $3d_{3/2}$ peaks at 280 and 282 eV, respectively, overlap the 1 s peaks of carbon in common carbon-related compounds (280–290 eV).[25] Thus the $RuCl_3$ should only have interactions with the Pd nanocrystals during the growth process. To depict the role of $RuCl_3$, we replaced $RuCl_3$ with either KCl or $CuCl_2$ while keeping other conditions unchanged, and this yielded nearly cubic nanocrystals (see Figure S4). Upon recognizing the importance of Ru^{3+} to tuning morphologies, it is imperative to elucidate why such guest cations can have a distinct effect on the development of Pd facets. Previously, it was reported that the addition of trace amounts of Cu^{2+} or Ag^+ cations can significantly alter the shapes and surface facets of noble metal nanocrystals such as platinum, silver, gold, and palladium, and an underpotential deposition (UPD) process is likely responsible for such a facet control.[26–29]

To better decode the mechanism, we have employed first-principles simulations to calculate the surface energies of Pd to reflect the relative stability of various Pd surface facets. In the simulations, we have considered several configurations for the chemisorbed Ru atoms with different atom proportions as shown in Figure 1 e. As a result, we can acquire the values for the surface energies of Ru-capped Pd surfaces in each configuration (see Table S1). In the case of pristine Pd surface growth, the surface energy for Pd{100} is 0.096 eV $Å^{-2}$, which is lower than that Pd{730} by 0.008 eV $Å^{-2}$. For this reason, the {100} facets are preferentially exposed on the Pd nanocrystals surface in the absence of Ru. Along with the implementation of Ru atoms on a Pd surface, both the Pd{100} and Pd{730} facets show gradually increased surface formation energy. However, the Pd{100} facet exhibits stronger dependence, thus leading to 0.020 eV $Å^{-2}$ higher than that for {730}. As a result, it can be predicted that the presence of Ru on a Pd{730} surface would make it much more favorable as compared with that of Pd{100}.

Following this mechanism, the Ru atoms which are formed on the nanocrystal surface, by quickly reducing Ru^{3+} cations, can substantially alter the surface energies to induce the formation of {730} facets in the synthesis. As Ru is a metal

with relatively high activity (redox potentials: Ru^{3+}/Ru 0.386 V versus SHE; $[PdCl_4]^{2-}/Pd$ 0.620 V versus SHE),[30] the deposited Ru will inevitably undergo galvanic replacement with the $[PdCl_4]^{2-}$ precursor during successive reactions. As such, no elemental Ru has been detected in the final products, similar to the reported cases of the UPD mechanism.[26–29] By capturing intermediate growth stages, we have observed the morphological evolution from cubic to concave profiles along with the size increase (see Figure S5). In particular, trace amounts of Ru are detectable in the intermediates, and gradually diminish as the growth proceeds (see Figure S6). This feature suggests that a UPD process may have occurred in the synthetic system, that is, generating Ru atoms on the surface to promote {730} facets and then removing them by galvanic replacement by $[PdCl_4]^{2-}$. In principle, other cations such as Cu^{2+} may play a similar role in altering surface energies.[26–29] However, the copper more easily forms alloys with Pd,[31] thus impeding the galvanic replacement of copper by $[PdCl_4]^{2-}$. The alloying between copper and Pd has been observed when the $CuCl_2$ is used in the synthesis (see Figure S4b).

It is worth pointing out that surface energy is not the only parameter determining the growth of nanocrystals, as kinetics may have huge impact on atomic addition in many cases. Recent work by Xia et al. reveals that surface diffusion is a critical process to the formation of concave surfaces, and can be tuned by kinetics, that is, the rates for atom deposition and surface diffusion ($V_{deposition}/V_{diffusion}$).[32] To depict the role of kinetics in our case, we have manipulated the $V_{diffusion}$ by adjusting synthesis temperatures, and it turns out that low $V_{diffusion}$ values at the reduced temperatures benefit the formation of concave surfaces (see Figure S7). Meanwhile, our measurements indicate that the addition of Ru^{3+} alters the kinetics of Pd precursor reduction and in turn increases the $V_{deposition}$ value (see Figure S8). Taken together, we can conclude that in our case kinetics ($V_{deposition}/V_{diffusion} > 1$) is a prerequisite to the formation process of concave surfaces in which Ru^{3+} makes an important contribution. This function of Ru^{3+} has been validated as a generic approach to concave structures including the seeding growth system (see Figure S9). Note that the etching process, another approach to concave structures,[33] is not likely responsible for the formation of concave surfaces in our case, as indicated by both nanocrystal morphological evolution (see Figure S5) and Pd(II) concentration reduction (see Figure S8).

In addition to facet control, particle size is another parameter characteristic to our synthetic system. The simulations indicate that the addition of Ru atoms increases the surface energies of Pd facets, thus providing a high-energy surface for atomic addition. As a result, most freshly formed Pd atoms prefer to add to the Pd nanocrystal surface for successive growth rather than self-nucleating, thus resulting in the significant increase in particle sizes. Figure 1 f shows the dependence of seed and particle numbers on the concentrations of added $RuCl_3$. It unambiguously affirms that the addition of $RuCl_3$ substantially reduces the number of seeds nucleated in solution. Thus the growth of nanocrystals prevails against the self-nucleation in the synthesis, which is the key to yielding larger final particles.

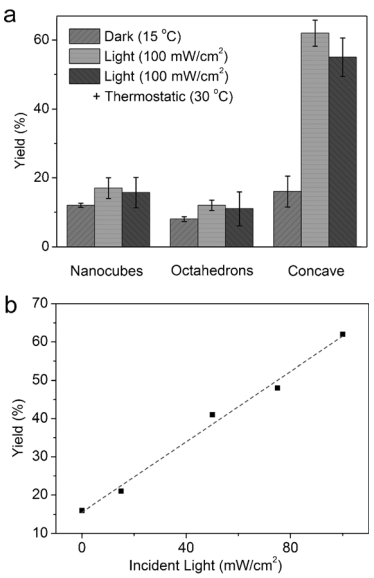

Figure 2. a) Catalytic hydrogenation of styrene catalyzed by various Pd nanocrystals under Xe-lamp full-spectrum light illumination (100 mW cm^{-2}, without or with thermostatic control) or in the dark. b) Yield of ethylbenzene catalyzed by the Pd nanostructures in Figure 1 c as a function of incident light intensity. Reaction conditions: 2 mmol styrene and 2 mg catalyst in 1 mL H_2O, 1-atm 10% H_2, no additional heating (room temperature: 15 °C), 1 h. The label "Concave" in Figures 2–4 denotes the sample shown in Figure 1 c.

The obtained Pd concave nanostructures offer desired particle sizes and surface structures for surface-plasmon-driven catalytic hydrogenation reactions. Figure 2 a shows the catalytic performance of our Pd concave nanostructures for styrene hydrogenation under different light conditions (also see Table S2), with reference to Pd nanocubes and octahedrons with comparable sizes (see Figure S10). In the dark at room temperature (15 °C), the Pd concave nanostructures show a yield of 16%, while those for nanocubes and octahedrons are 12 and 8%, respectively. The slightly better performance of concave structures can be ascribed to their larger portion of atoms at corner and edge sites, as these atoms are generally considered active sites for hydrogenation reactions.[13] Strikingly, the concave nanostructures exhibit dramatically improved performance under light illumination, benchmarked against their counterparts. The yield of ethylbenzene can be promoted from 16 to 62% with 100 mW cm^{-2} Xe-lamp full-spectrum light irradiation for the Pd concave nanostructures. In stark contrast, the yield enhancement is as low as 4–5% in the cases of Pd nanocubes and octahedrons. Figure 2 b shows that the hydrogenation reaction catalyzed by the concave nanostructures has nearly linear power law dependence on light intensities. It further confirms that the enhancement of catalytic performance occurs through light irradiation. Note that the nanostructures maintain their morphologies after the photodriven catalytic hydrogenation (see Figure S11).

To analyze the factors causing this performance difference, we first investigate the localized surface plasmon resonance (LSPR) properties of Pd nanostructures. Figure 3 a displays the UV/Vis extinction spectra of samples, which is

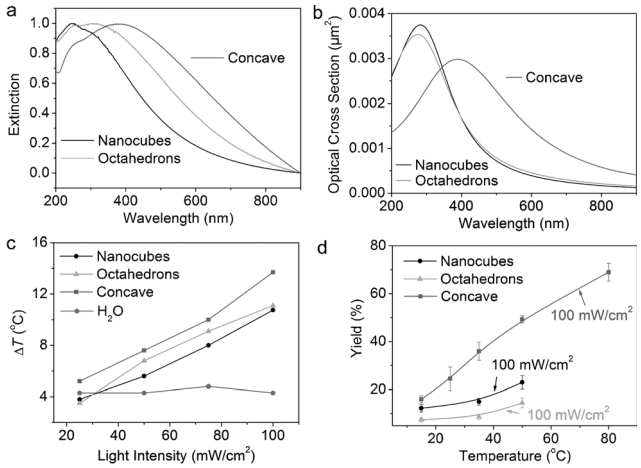

Figure 3. a) Normalized UV/Vis extinction spectra. b) Calculated absorption cross-sections of various Pd nanocrystals. In the DDA calculations, the incident light is directed along the direction normal to the flat face of a nanocrystal, and the edge lengths of nanocubes, octahedrons, and concave nanostructures are 35, 45 and 40 nm, respectively. c) Plots of temperature increase for aqueous suspensions of Pd nanocrystals at a concentration of 2 mg mL^{-1} as a function of light intensity (full-spectrum illumination time: 1 h). d) Yield of ethylbenzene from reaction catalyzed by the Pd nanostructures, in Figure 1c, as a function of temperature in dark. Reaction conditions: 2 mmol styrene and 2 mg catalyst in 1 mL H_2O, 1-atm 10% H_2, 1 h. The yields achieved by the Pd nanocrystals under 100 mW cm^{-2} full-spectrum illumination (the data in Figure 2a) are marked in the diagram as references.

compared with the calculated data using the discrete dipole approximation (DDA) method (Figure 3b). Although the three samples possess comparable absorption cross-sections at their LSPR peaks, the concave nanostructures exhibit much broader plasmonic band because of their lower shape symmetry, thus harvesting more visible light for catalytic reactions. As the UV light only accounts for 3% of the full spectrum Xe-lamp illumination in terms of power density (see Figure S12), absorbing light in the visible spectral range is greatly beneficial for efficiently coupling solar energy to the reaction system. The contribution of visible light to the reaction can be appreciated by analyzing the catalytic performance under different irradiation conditions. At the power density of 50 mW cm^{-2}, full-spectrum illumination gives a 41% yield while use of visible light ($\lambda > 400$ nm) can achieve 26% (see Table S3). By deducing the yield from the data for reaction in the dark (16%), one can see that the visible light roughly contributes to 40% the full-spectrum performance.

Photothermal effects converting light into heat are the most widely investigated factor for plasmonic-driven catalytic reactions.[14–17] To assess the photothermal effect on the reactions, we have measured the temperature increase in aqueous solution in the presence of various Pd nanostructures and full-spectrum irradiation (Figure 3c). The data indicate that higher solution temperature can be enabled by harvesting light in a broader spectral range with Pd concave nanostructures. To justify whether the photothermal effect on solution causes the catalytic performance difference, we performed the styrene hydrogenation at a set of different temperatures in the dark (see Table S4). As illustrated in Figure 3d, the yield when using the concave nanostructures under 100 mW cm^{-2} full-spectrum illumination is equivalent to that thermally driven at 70 °C, while at the same light intensity the nanocubes and octahedrons show catalytic efficiency comparable to that at about 40–45 °C in the dark. According to the temperature measurements, the photothermal effect should not make such a big difference in reaction solution temperature.

We have thus looked into some other possible factors. To ensure that thermal effect can be discounted, we employed a thermostatic device to maintain the reaction solution temperature at (30 ± 0.1) °C. As shown in Figure 2a, such temperature adjustments only reduces the yield by 7% for concave nanostructures. It suggests that other processes related to surface plasmon may also have made important contributions to catalytic performance improvement. In addition to the photothermal effect, the surface plasmon of metal nanocrystals generates hot electrons, which may have impact on specific catalytic reactions.[34] To assess whether the plasmonic hot electrons play a role, we performed a control experiment using the hybrid sample in which Pd concave nanostructures are supported on TiO_2 (Figure 4a). Upon

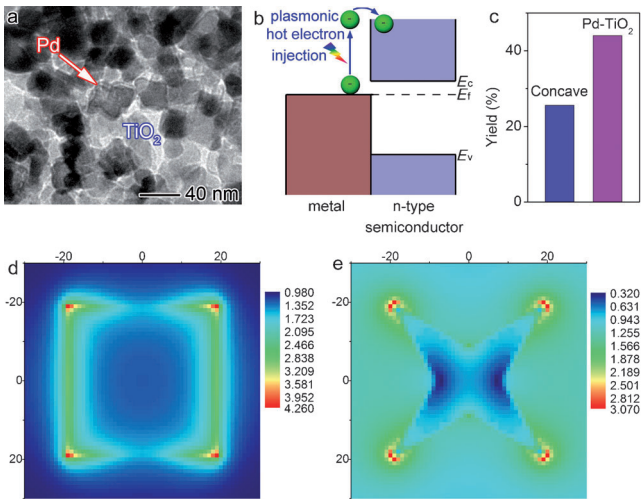

Figure 4. a) TEM image of Pd concave nanostructures supported on TiO_2. b) Illustration of the hot-electron transfer from Pd to TiO_2. c) Catalytic hydrogenation of styrene catalyzed by bare Pd concave nanostructures and those supported on TiO_2 using visible-light illumination ($\lambda > 400$ nm, 50 mW cm^{-2}). Reaction conditions: 2 mmol styrene and 2 mg catalyst in 1 mL H_2O, 1-atm 10% H_2, no additional heating (room temperature: 15 °C), 1 h. Plots of the relative field amplitude across the front (d) and middle (e) planes of a Pd concave nanostructure by DDA calculations. The calculation models are the same as those used for Figure 3b, and the incident light wavelengths are the LSPR band maxima in Figure 3b.

visible excitation, the hot electrons generated on the Pd can transfer to the conduction band of TiO_2 (Figure 4b),[35,36] thus reducing the effect of hot electrons on catalytic reactions. If the hot electrons made a positive contribution to the styrene hydrogenation, use of such a hybrid structure would result in

lower catalytic efficiency.[35] Figure 4c shows that the yield by the hybrid structure reaches 1.5 times that of a bare Pd concave sample (44% versus 26%) under 50 mW cm^{-2} visible-light illumination, thus indicating that the hot electrons are harmful to the styrene hydrogenation. Note that bare TiO_2 shows no catalytic reactivity under visible-light irradiation. This finding is further supported by theoretical simulations. In terms of hydrogenation reactions, dissociation of molecular H_2 and desorption of H_{ad} atoms from surface are often the rate-limiting steps.[2] In the specific case of Pd, it is known that the dissociation of molecular H_2 is a process easily occurring at the Pd surface nearly without an energy barrier.[37] Thus the desorption of H_{ad} atoms from the Pd surface holds the key to efficiently accomplishing hydrogenation reactions. We thus evaluate the effect of hot electrons on this desorption step by analyzing the adsorption energies of H atoms on the Pd surface by first-principles simulations (see Figure S13). To simplify the case, the adsorption energies are calculated when electrons are manually introduced onto the simulated Pd surface, thus reflecting the impact of hot electrons. As shown in Table S5, the binding of dissociated H atoms to the Pd surface is enhanced by the additional electrons, regardless of whether the H atoms are located on flat facets or corners and edges. The literature indicates that strong binding of hydrogen to metal sites is disadvantageous to hydrogenation.[2] As such, the simulation results here imply that the addition of negative charge (i.e., hot-electron injection) does not favor the hydrogenation reaction, aligning well with our experimental finding.

Upon excluding the hot-electron effect, we looked back at the structure characteristics of catalysts, and found that local heat generated on specific sites may contribute to the catalytic reaction. The plasmonic properties of metal nanoparticles can concentrate light at their surface (particularly at the apex of tips) and thus locally generate intensive heat.[34] When the nanoparticles are surrounded by solution, heat transfer takes place between the nanoparticles and the solution.[38] For this reason, the local temperature on the nanoparticle surface should be significantly higher than that measured in solution (Figure 3c). Based on the second law of thermodynamics, the heat capacity of Pd concave nanostructures is 22 mW while the nanocubes and octahedrons only offer 16 mW (Table S6). More importantly, the optical near-field enhancement responsible for local heat generation is more concentrated at the corners and edges of Pd nanocrystals as displayed in Figure 4d,e and Figure S14. The field amplitudes at these sites are comparable for all the three nanostructures at their LSPR band maxima. However, the concave nanostructures possess larger quantity of atoms around the corners and edges, thus providing more sites with local heat for the reaction. Given that hydrogenation mostly occurs at the corners and edges, the surface plasmon of concave nanostructures locally inducing high reaction temperature can more efficiently boost the hydrogenation yields.

In summary, we have developed a Ru^{3+}-mediated synthesis for the Pd concave nanostructures with desired size and surface structures. Enabled by their unique shape symmetry, the concave nanostructures can directly harvest UV-to-visible light for styrene hydrogenation, and their catalytic efficiency, using 100 mW cm^{-2} full-spectrum irradiation without additional heating, is comparable to that thermally driven at 70 °C. The superior photodriven catalytic performance to Pd nanocubes and octahedrons can be ascribed to a broad light-absorption band and large quantity of atoms on corner and edge sites. By excluding the hot-electron effect, we propose that the photothermal effect on solution temperature and local heat at the reaction sites may affect this surface plasmon-driven reaction process. This work opens up possibilities of utilizing solar energy instead of heat to drive organic reactions, and provides insights into the design of plasmonic catalytic materials.

Received: July 31, 2014
Published online: October 19, 2014

Keywords: heterogeneous catalysis · hydrogenation · nanostructures · palladium · surface plasmon resonance

[1] A. M. Smith, R. Whyman, *Chem. Rev.* **2014**, *114*, 5477.
[2] G. Kyriakou, M. B. Boucher, A. D. Jewell, E. A. Lewis, T. J. Lawton, A. E. Baber, H. L. Tierney, M. Flytzani-Stephanopoulos, E. C. H. Sykes, *Science* **2012**, *335*, 1209.
[3] S. Kidambi, J. Dai, J. Li, M. L. Bruening, *J. Am. Chem. Soc.* **2004**, *126*, 2658.
[4] O. M. Wilson, M. R. Knecht, J. C. Garcia-Martinez, R. M. Crooks, *J. Am. Chem. Soc.* **2006**, *128*, 4510.
[5] Y. Wang, J. Yao, H. Li, D. Su, M. Antonietti, *J. Am. Chem. Soc.* **2011**, *133*, 2362.
[6] Y. M. A. Yamada, Y. Yuyama, T. Sato, S. Fujikawa, Y. Uozumi, *Angew. Chem. Int. Ed.* **2014**, *53*, 127; *Angew. Chem.* **2014**, *126*, 131.
[7] T. Mitsudome, Y. Takahashi, S. Ichikawa, T. Mizugaki, K. Jitsukawa, K. Kaneda, *Angew. Chem. Int. Ed.* **2012**, *51*, 1481; *Angew. Chem.* **2012**, *124*, 1510.
[8] R. Narayanan, M. A. El-Sayed, *Nano Lett.* **2004**, *4*, 1343.
[9] H. Lee, S. Habas, S. Kweskin, D. Butcher, G. Somorjai, P. Yang, *Angew. Chem. Int. Ed.* **2006**, *45*, 7824; *Angew. Chem.* **2006**, *118*, 7988.
[10] R. Long, K. Mao, X. Ye, W. Yan, Y. Huang, J. Wang, Y. Fu, X. Wang, X. Wu, Y. Xie, Y. Xiong, *J. Am. Chem. Soc.* **2013**, *135*, 3200.
[11] C. Wang, H. Daimon, T. Onodera, T. Koda, S. Sun, *Angew. Chem. Int. Ed.* **2008**, *47*, 3588; *Angew. Chem.* **2008**, *120*, 3644.
[12] K. M. Bratlie, H. Lee, K. Komvopoulos, P. Yang, G. A. Somorjai, *Nano Lett.* **2007**, *7*, 3097.
[13] M. Crespo-Quesada, A. Yarulin, M. Jin, Y. Xia, L. Kiwi-Minsker, *J. Am. Chem. Soc.* **2011**, *133*, 12787.
[14] P. Christopher, H. Xin, S. Linic, *Nat. Chem.* **2011**, *3*, 467.
[15] P. Christopher, H. Xin, A. Marimuthu, S. Linic, *Nat. Mater.* **2012**, *11*, 1044.
[16] F. Wang, C. Li, H. Chen, R. Jiang, L. D. Sun, Q. Li, J. Wang, J. C. Yu, C. H. Yan, *J. Am. Chem. Soc.* **2013**, *135*, 5588.
[17] S. Sarina, H. Zhu, E. Jaatinen, Q. Xiao, H. Liu, J. Jia, C. Chen, J. Zhao, *J. Am. Chem. Soc.* **2013**, *135*, 5793.
[18] Y. Xiong, J. Chen, B. Wiley, Y. Xia, Y. Yin, Z. Li, *Nano Lett.* **2005**, *5*, 1237.
[19] M. Jin, H. Zhang, Z. Xie, Y. Xia, *Energy Environ. Sci.* **2012**, *5*, 6352.
[20] W. Niu, Z. Li, L. Shi, X. Liu, H. Li, S. Han, J. Chen, G. Xu, *Cryst. Growth Des.* **2008**, *8*, 4440.
[21] M. Rycenga, C. M. Cobley, J. Zeng, W. Li, C. H. Moran, Q. Zhang, D. Qin, Y. Xia, *Chem. Rev.* **2011**, *111*, 3669.

[22] B. Li, R. Long, X. Zhong, Y. Bai, Z. Zhu, X. Zhang, M. Zhi, J. He, C. Wang, Z. Y. Li, Y. Xiong, *Small* **2012**, *8*, 1710.
[23] M. Jin, H. Zhang, Z. Xie, Y. Xia, *Angew. Chem. Int. Ed.* **2011**, *50*, 7850; *Angew. Chem.* **2011**, *123*, 7996.
[24] Y. Bai, R. Long, C. Wang, M. Gong, Y. Li, H. Huang, H. Xu, Z. Li, M. Deng, *J. Mater. Chem. A* **2013**, *1*, 4228.
[25] C. D. Wanger, W. M. Riggs, L. E. Davis, J. F. Moulder, G. E. Muilenberg, *Handbook of X-Ray Photoelectron Spectroscopy*, PerkinElmer Corp., Eden Prairie, **1978**.
[26] H. Song, F. Kim, S. Connor, G. A. Somorjai, P. Yang, *J. Phys. Chem. B* **2005**, *109*, 188.
[27] M. L. Personick, M. R. Langille, J. Zhang, C. A. Mirkin, *Nano Lett.* **2011**, *11*, 3394.
[28] Y. Yu, Q. Zhang, J. Xie, J. Y. Lee, *Nat. Commun.* **2013**, *4*, 1454.
[29] A. R. Tao, P. Sinsermsuksakul, P. Yang, *Angew. Chem. Int. Ed.* **2006**, *45*, 4597; *Angew. Chem.* **2006**, *118*, 4713.
[30] R. C. Weast, *Handbook of Chemistry and Physics*, CRC Press, Boca Raton, FL, **1980**.
[31] Q. Cao, Y. M. Ju, D. An, M. R. Gao, J. W. Liu, C. H. Cui, S. H. Yu, *ChemSusChem* **2013**, *6*, 1878.
[32] X. Xia, S. Xie, M. Liu, H. C. Peng, N. Lu, J. Wang, M. J. Kim, Y. Xia, *Proc. Natl. Acad. Sci. USA* **2013**, *110*, 6669.
[33] H. Zhang, M. Jin, Y. Xia, *Angew. Chem. Int. Ed.* **2012**, *51*, 7656; *Angew. Chem.* **2012**, *124*, 7774.
[34] G. Baffou, R. Quidant, *Chem. Soc. Rev.* **2014**, *43*, 3898.
[35] S. Mukherjee, L. Zhou, A. M. Goodman, N. Large, C. Ayala-Orozco, Y. Zhang, P. Nordlander, N. J. Halas, *J. Am. Chem. Soc.* **2014**, *136*, 64.
[36] R. Long, K. Mao, M. Gong, S. Zhou, J. Hu, M. Zhi, Y. You, S. Bai, J. Jiang, Q. Zhang, X. Wu, Y. Xiong, *Angew. Chem. Int. Ed.* **2014**, *53*, 3205; *Angew. Chem.* **2014**, *126*, 3269.
[37] A. Maiti, R. Gee, R. Maxwell, A. Saab, *J. Phys. Chem. B* **2006**, *110*, 3499.
[38] N. J. Hogan, A. S. Urban, C. Ayala-Orozco, A. Pimpinelli, P. Nordlander, N. J. Halas, *Nano Lett.* **2014**, *14*, 4640.